Effects of Cellular Pharmacology on Drug Distribution in Tissues

Ronda K. Rippley and Cynthia L. Stokes
Department of Chemical Engineering, University of Houston, Houston, Texas 77204 USA

ABSTRACT The efficacy of targeted therapeutics such as immunotoxins is directly related to both the extent of distribution achievable and the degree of drug internalization by individual cells in the tissue of interest. The factors that influence the tissue distribution of such drugs include drug transport; receptor/drug binding; and cellular pharmacology, the processing and routing of the drug within cells. To examine the importance of cellular pharmacology, previously treated only superficially, we have developed a mathematical model for drug transport in tissues that includes drug and receptor internalization, recycling, and degradation, as well as drug diffusion in the extracellular space and binding to cell surface receptors. We have applied this "cellular pharmacology model" to a model drug/cell system, specifically, transferrin and the well-defined transferrin cycle in CHO cells. We compare simulation results to models with extracellular diffusion only or diffusion with binding to cell surface receptors and present a parameter sensitivity analysis. The comparison of models illustrates that inclusion of intracellular trafficking significantly increases the total transferrin concentration throughout much of the tissue while decreasing the penetration depth. Increasing receptor affinity or tissue receptor density reduces permeation of extracellular drug while increasing the peak value of the intracellular drug concentration, resulting in "internal trapping" of transferrin near the source; this could account for heterogeneity of drug distributions observed in experimental systems. Other results indicate that the degree of drug internalization is not predicted by the total drug profile. Hence, when intracellular drug is required for a therapeutic effect, the optimal treatment may not result from conditions that produce the maximal total drug distribution. Examination of models that include cellular pharmacology may help guide rational drug design and provide useful information for whole body pharmacokinetic studies.

INTRODUCTION

Accurate delivery of therapeutic drugs to the appropriate tissues is necessary to maximize efficacy of treatment and minimize harmful side effects in non-diseased tissues. The advent of monoclonal antibody technology motivated the idea that tissues might be selectively targeted by macromolecular drugs, a new approach to disease detection and treatment. Targeted drug delivery strategies have numerous potential applications, including cancer detection and treatment (LoBuglio and Saleh, 1992), anti-growth factor receptor therapy (Mulshine et al., 1992), and gene therapy (Chen et al., 1994). However, physiological complications can preclude the in vivo efficacy of therapeutics that are successful in vitro. Often, a drug is ineffective in vivo because it reaches the target tissue in insufficient quantities for a number of reasons (Jain, 1989; Weinstein et al., 1987; Epstein and Khawli, 1991). Drug may be degraded before reaching the diseased tissue, or drug transport across capillaries into surrounding tissue may be restricted (Jain, 1989). Drug that does access the tissue may be degraded by cells nearest the blood vessels before it can reach interior target cells (Jain, 1994). In addition, transport of macromolecular drugs in tumors may be impeded by interstitial fluid pressure gradients (Boucher et al., 1990) or by specific binding to surface receptors on cells near blood vessels (Juweid et al., 1992).

In this work, we are interested in the processes that govern the distribution of drug within a tissue once the drug reaches that tissue. Factors that determine drug access to and specificity for the desired target tissue include physicochemical factors and cellular pharmacology (Jain, 1989; van Osdol et al., 1991; Epstein and Khawli, 1991; Stein and Cheng, 1993). The diffusive and convective transport of drug throughout the target tissue is governed by vascular permeability, tissue heterogeneity, convection of interstitial fluid, drug diffusivity, and interstitial fluid pressure. The cellular pharmacology, which includes drug/receptor binding at the cell surface, internalization, and intracellular routing, determines the drug interaction with the tissue cells. Simple delivery of drug to a tissue may be inadequate for therapy, however, because the actions of many drugs such as immunotoxins, hormonotoxins, and oligonucleotides require intracellular access (Olsnes et al., 1989; Stein and Cheng, 1993, Preijers et al., 1988). Consequently, several current approaches to drug design attempt to achieve entry into cells by exploiting receptor-mediated processes. Monoclonal antibody/drug conjugates can be directed against disease-specific cell surface receptors, e.g., tumor markers such as melanoma-associated antigen (LoBuglio and Saleh, 1992). Receptors for growth factors, transferrin, and low density lipoprotein are often overexpressed in malignant tissues (Vitetta et al., 1993; Thorstensen and Romslo, 1993; Firestone, 1994) and hence make good targets for high affinity drugs. To take advantage of receptors for molecules that are required for cell growth, some strategies involve

Received for publication 24 March 1995 and in final form 31 May 1995.
Address reprint requests to Dr. Cynthia Stokes, Department of Chemical Engineering, University of Houston, 4800 Calhoun, Room S222D, Houston, TX 77204-4792. Tel.: 713-743-4309; Fax: 713-743-4323; E-mail: stokes@uh.edu

0006-3495/95/09/825/15 $2.00

conjugates of toxins to anti-transferrin receptor antibodies (Martell et al., 1993), anti-growth factor receptor antibodies (Kim et al., 1993; Hirota et al., 1989) or natural receptor ligands such as hormonal growth factors (Vitetta et al., 1993; Schwartz et al., 1987) and low density lipoprotein (Firestone, 1994). Unfortunately, a further complication is that internalization of drug may be necessary but insufficient for efficacy. For instance, cytotoxicity may be dependent on the rates of specific cellular drug processing and routing steps (Akhtar and Juliano, 1992; Wargalla and Reisfeld, 1989; Byers et al., 1991; May et al., 1991).

The large number of transport and pharmacological parameters that influence drug distribution in a tissue and the difficulty of measuring drug distributions in animal systems encumber in vivo study of targeted drug delivery (Leichner et al., 1990). The complexity of the problem has attracted mathematical analyses. Previous models have examined targeted drug delivery using the paradigm of monoclonal antibody uptake by a tumor. Compartmental pharmacokinetic models describe average drug concentrations in the plasma, target tissue, and organs such as the liver and kidneys (e.g., Sung et al., 1992; Thomas et al., 1989). These models lump together such processes as reversible drug binding and drug endocytosis and metabolism into one process, described by a single rate parameter. A major limitation of lumped parameter models, the lack of spatial drug distribution information, is rectified by distributed parameter models (e.g., Baxter and Jain, 1991; McFadden and Kwok, 1988). The latter provide drug concentration profiles in the target tissue and have been used to study the effects of interstitial fluid flow and pressure on drug distribution (Baxter and Jain, 1991). Other models have combined the salient aspects of global compartmental pharmacokinetics and distributed parameter models to consider the impact of treatment protocols, capillary permeability, lymphatic efflux, and other binding and transport parameters (e.g., van Osdol et al., 1991, 1993; Baxter et al., 1992). The cellular internalization and trafficking of drug, however, were accounted for by a single metabolism rate constant.

In this paper, we describe a mathematical model that explicitly includes the cellular pharmacology to explore its effects on drug distribution in a model tissue. The model combines drug transport and specific, saturable binding processes with descriptions of drug and receptor internalization and trafficking. Our goal is to predict whether cellular pharmacology has a significant impact on drug transport and distribution in tissues and, if so, what cellular processes might be targeted in rational design of therapeutics to maximize efficacy. We have used the model to examine the impact of cellular pharmacology on the distribution of transferrin in a tissue expressing the transferrin receptor. We chose transferrin and its receptor as the model system because this receptor is often overexpressed in malignant tissues (Thorstensen and Romslo, 1993) and therefore has diagnostic and therapeutic potential. In fact, the transferrin receptor has been a target for immunotoxin therapy of cancer (Pirker et al., 1985), delivery of drugs across the blood-brain barrier (Yoshikawa and Pardridge, 1992), and gene therapy (Citro et al., 1992; Cotten et al., 1990). In addition, the endocytic cycle of transferrin via the transferrin receptor is well characterized in a number of cell lines (Ciechanover et al., 1983; Cain et al., 1991; Klausner et al., 1983), and so the binding, internalization and recycle rate constants are available for use in the model. Our results predict that cellular pharmacology strongly affects the distribution of transferrin in tissue. One important observation is that the total tissue concentration of transferrin (extracellular plus cell-associated) does not necessarily predict intracellular transferrin levels, demonstrating that total drug concentration may not be a sufficient indicator of drug efficacy. In addition, increasing receptor density or receptor/transferrin affinity impedes transferrin penetration in the tissue and gives rise to an "internal trapping" of transferrin near the source. This may be the actual cause of the experimentally observed "binding site barrier" (Fujimori et al., 1989) for ligands that are internalized.

MATHEMATICAL MODEL AND METHODS

Cellular pharmacology model

We have developed a cellular pharmacology model that describes the local pharmacokinetics of a macromolecular drug in tissue. In this work we apply the model to a specific cell type and receptor/ligand system relevant to targeted drug delivery. We include extracellular diffusive drug transport, specific reversible binding of drug to cell surface receptors, and a detailed consideration of receptor-mediated endocytosis and trafficking of drug. We neglect contributions of convection in this treatment, as our primary goal is to assess the impact of endocytosis and intracellular trafficking on drug distribution. The tissue is modeled as a continuum. The various chemical species (e.g., cell surface receptors, intracellular ligand, etc.) in the tissue are modeled as spatially continuous variables; discrete cells are not explicitly considered. Rather, each cell-associated species is treated as a continuous variable in space, but is spatially immobile. Only unbound extracellular drug is free to diffuse. The discretization of the model for computer simulation does, however, provide a spatial aspect to the cells as described below. A schematic representation of the model system is shown in Fig. 1. We impose cylindrical geometry on the tissue, and the model is constrained to one dimension. Drug concentration in the blood plasma is time-dependent. Access of drug to the tissue is governed by capillary permeability. Extravascular drug diffuses away from the capillary wall ($r = 0$) through the extracellular space (Fig. 1 *a*), and the model assumes that there is no flux of drug at the boundary $r = R$. Drug binds to cell surface receptors and may be internalized, recycled to the cell surface, and/or released back into the extracellular space (Fig. 1 *b*). In the general model, as indicated in Fig. 1 *b*, internalized drug and receptors can be degraded in lysosomes, and the surface receptor pool can be replenished by synthesis of new recep-

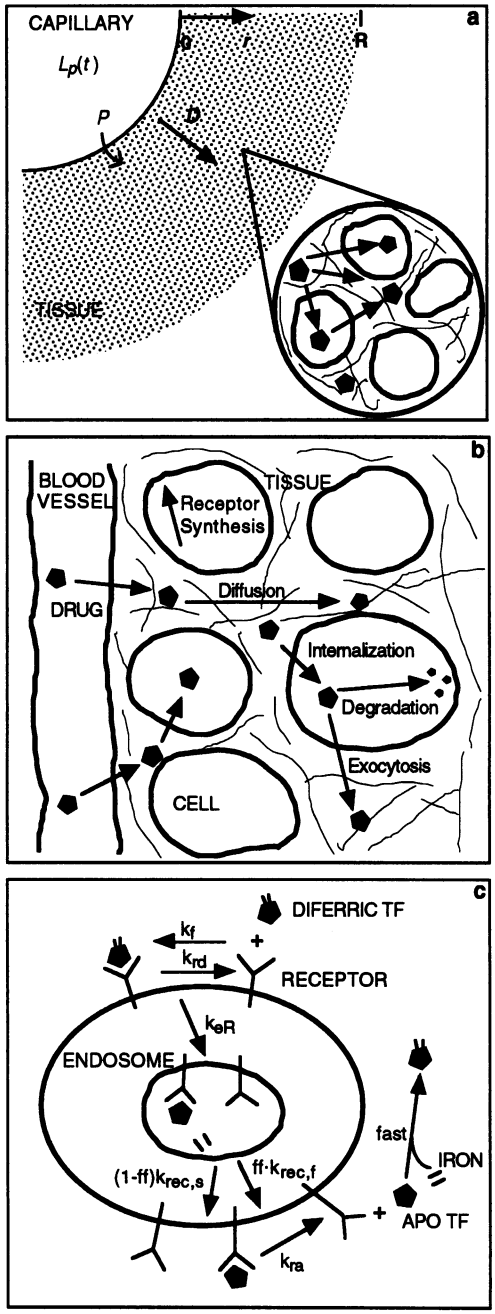

FIGURE 1 Schematic representation of the cellular pharmacology model. (*a*) Model geometry. The function $L_p(t)$ is given by Eq. 7 and represents the concentration of transferrin present in the blood plasma. The flux of drug across the capillary wall is related to capillary permeability P by Eq. 8. The drug may diffuse through the extracellular space of the tissue with effective diffusion coefficient D, and may also interact with the cells as shown in the inset. (*b*) Processes included in the general cellular pharmacology model. Pentagons represent drug molecules. (*c*) Schematic representation of a single CHO TfT1.11 cell and the specific transferrin/CHO cell interactions included in the transferrin adaptation of the cellular pharmacology model. The rate constants are defined in Table 1.

tors. However, these processes are not considered in this work for reasons stated below. We omit nonspecific internalization of drug (fluid phase uptake), as it is considered insignificant for extracellular drug concentrations $<10^{-8}$ M (Lauffenburger and Linderman, 1993). We illustrate concentration profiles for distances up to 1.0 mm from the capillary wall. The very short distances (a few hundred micrometers) may be relevant to established vascularized tumors, whereas greater depths may be relevant for early avascular tumors that can be several millimeters in diameter before neovascularization occurs. Possible sinks such as lymphatics are not considered in this initial study.

The cellular pharmacology model includes a reaction-diffusion equation for extracellular ligand concentration and a basic model for trafficking as described by Lauffenburger and Linderman (1993). In this study, we apply the general model to the specific system of transferrin and its receptor in the Chinese hamster ovary mutant cell line TfT1.11 (Cain et al., 1991). Fig. 1 *c* is a schematic representation of the endocytosis and trafficking portion of the model that illustrates the application of the cellular pharmacology model to the transferrin system and TfT1.11 cells. We use aspects of a kinetic model of the transferrin cycle proposed by Ciechanover et al. (1983). Qualitatively similar models of the transferrin cycle in human leukemic K562 cells and mouse teratocarcinoma stem cells have been described (Klausner et al., 1983; Karin and Mintz, 1981). Ciechanover et al. (1983) based their model on experimental evidence in the human hepatoma cell line HepG2 (Dautry-Varsat et al., 1983) that transferrin and its receptor remain associated during the endocytosis cycle, and no degradation of the transferrin receptor occurs over short periods (hours). The transferrin cycle model assumes that no synthesis of new receptors occurs over similar time periods. Ciechanover et al. (1983) observed that endosomal receptor-transferrin complexes contain apotransferrin, and surface complexes contain either ferrotransferrin or apotransferrin. Trace amounts of iron in the surrounding medium are sufficient to rapidly convert all apotransferrin to ferrotransferrin as it dissociates from cell surfaces (Dautry-Varsat et al., 1983), and so all free transferrin is considered to be ferrotransferrin. Throughout the paper, we use the term transferrin as a catch-all term that is inclusive of both transferrin species, but it is understood that, unless otherwise specified, intracellular transferrin is in apo form, extracellular transferrin is in diferric form, and the surface pool of receptor/transferrin complexes contains both diferric and apo forms. The dissociation of ferrotransferrin and apotransferrin from surface receptors is governed by distinct rate constants (Klausner et al., 1983; Dautry-Varsat et al., 1983). Because the transferrin receptor is considered to reside in coated pits whether bound to ligand or not, there is no alteration of receptor internalization rate resulting from ligand binding (Lauffenburger and Linderman, 1993). We also incorporate experimental evidence (Cain et al., 1991) that TfT1.11 cells have two recycle pathways that are distinguished by markedly different rates.

The equations that describe the cellular pharmacology model as applied to the transferrin cycle in TfT1.11 cells are

as follows. Extracellular transferrin concentration L (M) is given by:

$$\frac{\partial L}{\partial t} = \frac{D}{r}\left(\frac{\partial}{\partial r}\left(r\frac{\partial L}{\partial r}\right)\right) - k_f R_s L \frac{n_v}{N_{Av}} + k_{ra} C_{sa} \frac{n_v}{N_{Av}} + k_{rd} C_{sd} \frac{n_v}{N_{Av}} \quad (1)$$

The surface receptor complexes with diferric and apotransferrin, C_{sd} ($\# \cdot \text{cell}^{-1}$) and C_{sa} ($\# \cdot \text{cell}^{-1}$), respectively, change with time as:

$$\frac{\partial C_{sd}}{\partial t} = k_f R_s L - k_{rd} C_{sd} - k_{eR} C_{sd} \quad (2)$$

$$\frac{\partial C_{sa}}{\partial t} = -k_{ra} C_{sa} + [k_{rec,f} ff + k_{rec,s}(1 - ff)] C_i - k_{eR} C_{sa} \quad (3)$$

Surface free receptors R_s ($\# \cdot \text{cell}^{-1}$) change with time as:

$$\frac{\partial R_s}{\partial t} = -k_f R_s L + k_{ra} C_{sa} + k_{rd} C_{sd} - k_{eR} R_s + [k_{rec,f} ff + k_{rec,s}(1 - ff)] R_i \quad (4)$$

The time rates of change of intracellular receptor/transferrin complexes C_i ($\# \cdot \text{cell}^{-1}$) and intracellular free receptors R_i ($\# \cdot \text{cell}^{-1}$) are:

$$\frac{\partial C_i}{\partial t} = k_{eR}(C_{sa} + C_{sd}) - [k_{rec,f} ff + k_{rec,s}(1 - ff)] C_i \quad (5)$$

$$\frac{\partial R_i}{\partial t} = k_{eR} R_s - [k_{rec,f} ff + k_{rec,s}(1 - ff)] R_i \quad (6)$$

Table 1 summarizes the definitions of variables and parameters and provides base case values for the kinetic rate constants and other parameters associated with the model equations. The k values represent specific rate constants: k_f ($\text{M}^{-1}\ \text{s}^{-1}$) is the forward binding rate constant for cell surface receptor/transferrin binding; k_{rd} (s^{-1}) and k_{ra} (s^{-1}) are reverse binding rate constants for diferric and apotransferrin, respectively; k_{eR} (s^{-1}) is the rate constant for internalization of both free surface receptors and surface receptor/transferrin complexes; and $k_{rec,f}$ (s^{-1}) and $k_{rec,s}$ (s^{-1}) are the rate constants for the fast and slow recycle pathways, respectively. n_v ($\text{cell} \cdot l^{-1}$) is the cell number density in the tissue. N_{Av} (mol^{-1}) is Avogadro's number. ff is the fraction of internalized receptor/transferrin complexes that is recycled through the fast pathway. D ($\text{cm}^2 \cdot \text{s}^{-1}$) is the effective diffusion coefficient.

We model the ferrotransferrin source in the plasma as an intravenous bolus dose of drug. To simulate the serum pharmacokinetics of known macromolecular therapeutics, we chose parameters measured for the biexponential decay of the plasma concentration of radiolabeled $F(ab')_2$ in humans (Fujimori et al., 1989). IgG $F(ab')_2$ is a glycoprotein similar in molecular weight to ferrotransferrin.

TABLE 1 Definition of variables and parameters with base case parameter values used in the cellular pharmacology model

Symbol	Definition	Value
C_i (M)	Intracellular transferrin	
C_{sa} ($\#\cdot\text{cell}^{-1}$)	Surface receptor/apotransferrin complexes	
C_{sd} ($\#\cdot\text{cell}^{-1}$)	Surface receptor/diferric transferrin complexes	
$\overline{C_i}$ (M)	Spatially averaged intracellular transferrin	
D ($\text{cm}^2\cdot\text{s}^{-1}$)	Effective diffusion coefficient	2×10^{-8}
ff	Fraction of internal receptors and complexes recycled in fast pathway	0.815*
k_{eR} (s^{-1})	Internalization rate constant	3.333×10^{-3}‡
k_f ($\text{M}^{-1}\cdot\text{s}^{-1}$)	Transferrin/receptor association rate constant	5×10^{4}‡
k_{rd} (s^{-1})	Transferrin/receptor dissociation rate constant for diferric transferrin	1.667×10^{-3}‡
k_{ra} (s^{-1})	Transferrin/receptor dissociation rate constant for apotransferrin	4.333×10^{-2}‡
$k_{rec,f}$ (s^{-1})	Fast recycle pathway rate constant	1.359×10^{-3}*
$k_{rec,s}$ (s^{-1})	Slow recycle pathway rate constant	9.62×10^{-5}*
L (M)	Extracellular transferrin	
$\overline{L}$ (M)	Spatially averaged extracellular transferrin	
L_0 (M)	Initial plasma transferrin concentration	2.0×10^{-8}
L_p (M)	Plasma transferrin concentration	
N_{Av} (mol^{-1})	Avogadro's number	6.022×10^{23}
n_v ($\text{cell}\cdot l^{-1}$)	Cell number density	1.0×10^{12}
P ($\text{cm}\cdot\text{s}^{-1}$)	Transferrin capillary permeability	9.0×10^{-7}§
R_i ($\#\cdot\text{cell}^{-1}$)	Intracellular free receptors	
R_s ($\#\cdot\text{cell}^{-1}$)	Surface free receptors	
R_T ($\#\cdot\text{cell}^{-1}$)	Receptor density	1.6×10^{5}¶
Tf_{tca} (M)	Total cell-associated transferrin	
Tf_{tot} (M)	Total tissue transferrin	
$\overline{Tf_{tot}}$ (M)	Spatially averaged total tissue transferrin	
α_1	Pharmacokinetic pre-exponential factor	0.61‖
α_2	Pharmacokinetic pre-exponential factor	0.39‖
λ_1 (s^{-1})	Pharmacokinetic time constant	1.5×10^{-4}‖
λ_2 (s^{-1})	Pharmacokinetic time constant	6.3×10^{-6}‖

* Data for 33°C; Cain et al., 1991; ‡ Ciechanover et al., 1983; § Baxter et al., 1992; ‖ Fujimori et al., 1989; ¶ Klausner et al., 1984.

The equation for the plasma ferrotransferrin concentration L_p is:

$$L_p = L_0\{\alpha_1 \exp(-\lambda_1 t) + \alpha_2 \exp(-\lambda_2 t)\} \quad (7)$$

where α_1, λ_1, α_2, and λ_2 are fitted constants (Table 1), and L_0 is defined as a typical initial bolus intravenous dose. We require two boundary conditions and the initial condition to specify the transferrin system application of our model. Transferrin flux from the capillary into the tissue is related to capillary permeability and the transferrin gradient across the capillary wall:

$$-D\frac{\partial L}{\partial r}\bigg|_{r=0} = P(L_p - L|_{r=0}) \quad (8)$$

where P ($\text{cm} \cdot \text{s}^{-1}$) is the capillary permeability coefficient. We assume no flux of transferrin at $r = \text{R}$ due to symmetry

with tissue surrounding adjacent capillaries, and thus the second boundary condition is:

$$\frac{\partial L}{\partial r} = 0 \quad \text{at} \quad r = \mathrm{R} \tag{9}$$

Initially, there is no transferrin in the tissue and for all r:

$$L(r, 0) = 0$$
$$C_i(r, 0) = 0$$
$$C_{sa}(r, 0) = 0 \tag{10a–d}$$
$$C_{sd}(r, 0) = 0$$

Ciechanover et al. (1983) determined that HepG2 cells expressed only one-third of their total receptors on the surface and kept two-thirds in intracellular locations, so we specify the initial condition for R_s and R_i as:

$$R_s(r, 0) = 0.333R_T$$
$$R_i(r, 0) = 0.667R_T \tag{10e–f}$$

where R_T (# · cell^{-1}) is the total number of transferrin receptors.

The model equations were made dimensionless with appropriate scaling to identify groups of parameters that have similar effects. The results are presented in dimensional form, however, to provide a meaningful spatiotemporal context. The results of parameter variation are organized in sections representative of given dimensionless groups. Parameter variations were performed with constant affinity, i.e., $k_{ra} = k_{rd}$, as explained in the Results section.

The volume that cells occupy is not obvious in the continuous equations above (Eqs. 2–6). The discretized equations for numerical simulation, however, have a spatial step size of 10 μm, on the order of a cell diameter. In this discrete sense, each cell layer is 10 μm thick and consists of an extracellular space and a cellular compartment to which ligands can bind and be internalized and recycled. Extracellular ligand is exchanged between the extracellular compartments of adjacent cell layers via diffusive flux, and cell-associated ligand can dissociate from a cell into the extracellular compartment surrounding that cell.

Diffusion-only model

We modeled tissue transferrin distribution resulting from diffusive transport alone using Eq. 1 with the same boundary conditions and initial condition. For this case, k_f, k_{ra}, and k_{rd} were set equal to zero.

Diffusion-with-surface-binding model

We considered the effect of transferrin binding to cell surface receptors without inclusion of cell trafficking rate processes by solving the cellular pharmacology model with the following changes. k_{eR} was set equal to 0. We chose a receptor density R_T (# · cell^{-1}) of 40,000, the steady state value of R_s observed in base case simulations of the cellular pharmacology model. For the transferrin base case, we required 69% of the surface transferrin to dissociate from receptor as apotransferrin with rate constant k_{ra}, while the remaining 31% dissociated as ferrotransferrin with k_{rd}. (An analysis of the actual binding and internalization rate constants shows that, if internalization and recycle are considered, 69% of initially surface-bound ferrotransferrin is internalized before it can dissociate from surface receptors, and thus that percent dissociates as apotransferrin with k_{ra} while the remaining 31% dissociates with k_{rd}. This has been demonstrated experimentally in HepG2 cells (Ciechanover et al., 1983).) To generalize the comparison among models, the diffusion-with-binding case was also simulated with constant affinity ($k_{ra} = k_{rd}$) for both normal diferric transferrin/receptor affinity (3×10^7 M^{-1}, referred to as the constant affinity base case) and higher affinity (10^9 M^{-1}). These simulations were compared with analogous cellular pharmacology simulations.

Other calculated quantities

Extracellular and intracellular transferrin concentrations were calculated as functions of time and space. Total tissue transferrin (apo plus ferro) concentration is a sum of intracellular, surface-bound, and extracellular transferrin:

$$Tf_{tot} = L + C_{sa} + C_{sd} + C_i \tag{11}$$

Total cell-associated transferrin (apo plus ferro) concentration is the sum of intracellular and cell surface transferrin concentrations:

$$Tf_{tca} = C_{sa} + C_{sd} + C_i \tag{12}$$

Additionally, the spatially averaged total, intracellular, and extracellular transferrin concentrations were calculated as the arithmetic averages of these concentrations to a distance of 3 mm from the capillary wall and are denoted $\overline{Tf_{tot}}$, $\overline{C_i}$, and $\overline{L}$, respectively.

Numerical solution method

Eqs. 1–10 were dedimensionalized and integrated numerically to calculate the distribution of extracellular and cell-associated transferrin throughout the tissue for up to 96 h. A fourth-order Runge-Kutta method (Press et al., 1989) was used to integrate the kinetic balance equations (Eqs. 2–6). Calculation of the spatial profile from Eq. 1 at each time was simplified by offsetting the time step for this equation by one-half time step from that of Eqs. 2–6. This makes Eq. 1 linear, because all variables except L are treated as constants equal to the values calculated from Eqs. 2–6 at the previous half time step. The Crank-Nicholson scheme (Davis, 1984) was used to obtain the spatial solution for L from Eq. 1 at each time step. All calculations were per-

formed in double precision using FORTRAN 77 on a Hewlett Packard (Palo Alto, CA) 9000 series Apollo 720 workstation. Spatial and temporal step sizes were 0.001 cm and 25 s, respectively. No improvement of resolution was achieved for smaller step sizes. The maximum radius of tissue simulated was 3 mm.

Parameter values

Table 1 contains the parameter values used for the transferrin base case calculation. These values are used throughout except where changes are noted. The binding and internalization rate constants were taken from experimental literature for the transferrin cycle in HepG2 cells (Ciechanover et al., 1983). The recycling rate constants are for CHO TfT1.11 cells at 33°C and were taken from Cain et al. (1991). The receptor density is that of wild-type CHO as well as TfT1.11 at 33°C and was taken from Klausner et al. (1984). The pharmacokinetic rate constants for drug degradation in the plasma were taken from Fujimori et al. (1989) as explained with Eq. 7. D, the effective diffusion coefficient, was estimated by determining the scaling factor for diffusion of transferrin and IgG in dilute solution using a relation for dilute solution diffusivity (McCabe et al., 1985). We assumed that the scale factor applies in tissue as well as dilute solution, and scaled a value of D measured for IgG in tumors (Jain, 1990). The cell number density, n_v, was estimated to be 10^{12} cells $\cdot\, l^{-1}$, a typical tissue cell density. Capillary permeability, P, was assumed to be similar to that for $F(ab')_2$ and was taken from Baxter et al. (1992). A reasonable therapeutic peptide concentration was chosen for L_0, the initial plasma concentration of transferrin.

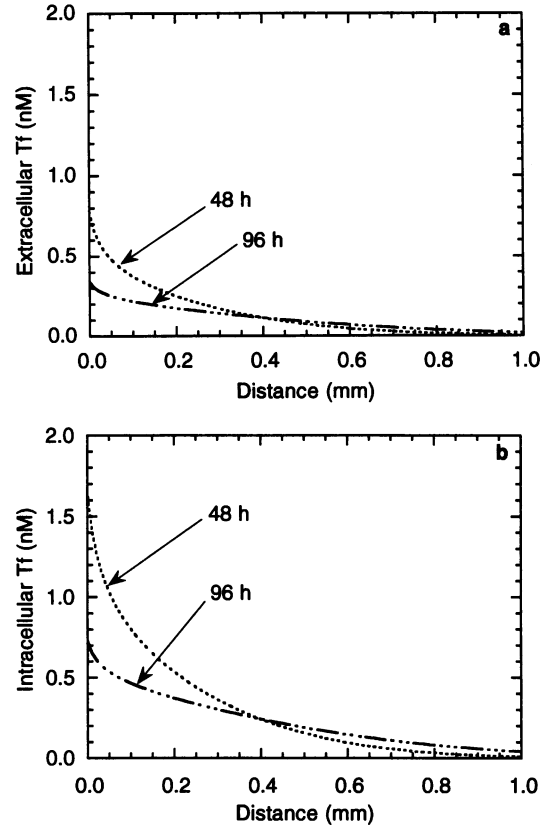

FIGURE 2 Results of base case simulations for the cellular pharmacology model. Spatial distribution of (*a*) extracellular transferrin L and (*b*) intracellular transferrin C_i at 48 h and 96 h. Parameter values are given in Table 1.

RESULTS

Base case calculations

The cellular pharmacology model (Eqs. 1–10) was simulated with the base case parameter values for transferrin given in Table 1. Spatial profiles of extracellular (L) and intracellular (C_i) transferrin concentrations at 48 and 96 h are plotted in Fig. 2. Both panels indicate that broadening and flattening of the transferrin profile occur over time. After very early times (minutes), intracellular transferrin concentrations are higher than extracellular transferrin concentrations throughout the tissue as shown here, illustrating a substantial retention of ligand by the cells.

We investigated whether including cellular pharmacology affected the transferrin distribution by comparing the cellular pharmacology model to models that considered only diffusion of transferrin in the extracellular space (diffusion-only model) or diffusion with reversible binding to cell surface receptors (diffusion-with-binding model). Fig. 3 *a* gives the spatial distribution of total transferrin Tf_{tot} for each model at 48 h. Transferrin/cell interactions clearly affect the amplitude of the total transferrin profile. The cellular pharmacology model predicts a dramatic increase in amplitude in comparison with the diffusion-only case, whereas the diffusion-with-binding model predicts only a slight increase in amplitude for the same parameter set. Also, the addition of rate processes associated with transferrin internalization and intracellular trafficking results in reduced penetration of transferrin into the tissue. Fig. 3 *b* shows the temporal distribution of average total transferrin concentration $\overline{Tf_{tot}}$ given by each of the three models. The cellular pharmacology model gives the highest $\overline{Tf_{tot}}$ at all times, while the diffusion-with-binding model has a $\overline{Tf_{tot}}$ profile that is very similar to the diffusion-only model. Included on Fig. 3 *b* is a plot of the average intracellular transferrin concentration $\overline{C_i}$ as determined by the cellular pharmacology model. From this curve, it is clear that much of the transferrin present in the tissue at any given time is in the intracellular pool. Because the diffusion-with-binding model does not account for internalized transferrin, the uptake and retention of transferrin are grossly underestimated by that model for these parameter values.

The presence of cells also has a marked impact on the distribution of free transferrin. Fig. 3 *c* gives the spatial distribution of extracellular transferrin L for the three models at 48 h. At most points, the extracellular transferrin concentration and penetration depth are largest for diffusion

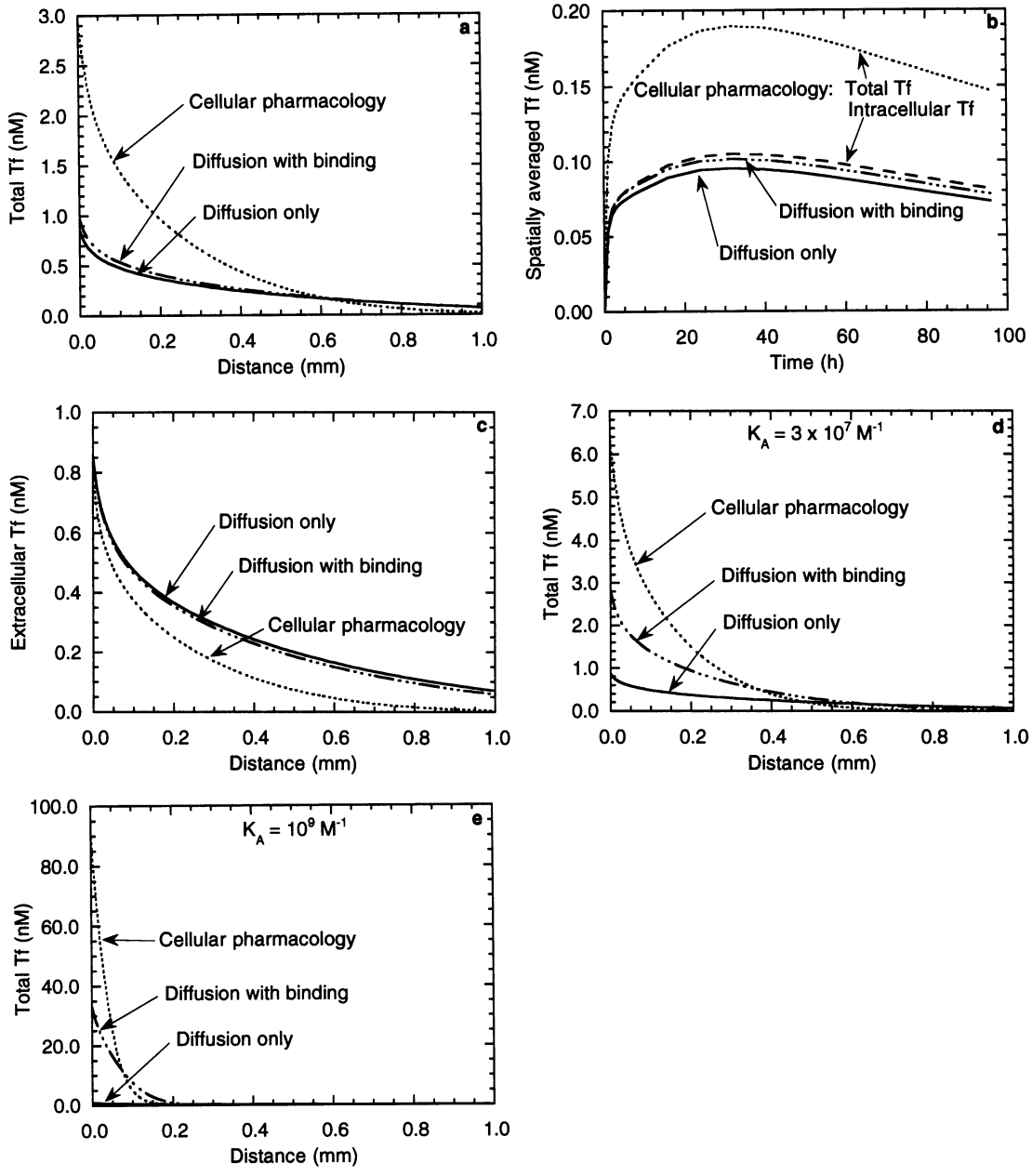

FIGURE 3 Comparison of transferrin base case (*a–c*), constant affinity base case (*d*), and constant high affinity (*e*) simulations for the cellular pharmacology, diffusion-with-binding, and diffusion-only models. Note that the ordinates have different scales. (*a*) Spatial distribution of total transferrin Tf_{tot} (extracellular plus cell-associated) at 48 h. (*b*) Temporal distribution of spatially averaged total transferrin $\overline{Tf_{tot}}$. Also shown is the temporal distribution of average intracellular transferrin $\overline{C_i}$ calculated using the cellular pharmacology model. This illustrates that much of the transferrin is intracellular in the cellular pharmacology model. Spatially averaged quantities represent the arithmetic average in a depth of tissue up to 3 mm from the source. (*c*) Spatial distribution of extracellular transferrin L at 48 h. (*d*) Spatial distribution of total transferrin Tf_{tot} at 48 h for $K_A = 3 \times 10^7\ M^{-1}$, which is the K_A when the reverse binding constant is the same for apo and diferric transferrin. (*e*) Spatial distribution of total transferrin Tf_{tot} at 48 h for $K_A = 10^9\ M^{-1}$ ($k_f = 10^5\ M^{-1}\ s^{-1}$, $k_{rd} = 10^{-4}\ s^{-1}$). The diffusion-only curve (*solid line*) is the same as in *d*.

alone, and nearly as great for diffusion with surface binding. However, though the amplitude of L is unchanged, the penetration depth is greatly reduced when cellular pharmacology is considered. Consideration of Fig. 3, *a–c*, reveals that the penetration ability of transferrin is compromised by the addition of rate processes associated with cells, and inclusion of the detailed cell biology causes tissue retention and uptake of transferrin that are much greater than predicted by diffusion with surface binding alone.

It is important to note that in the transferrin cycle the transition from diferric to apotransferrin during internalization and recycle causes a shift from a slower to a faster rate of dissociation of transferrin from the cell surface. Accordingly, both the cellular pharmacology and diffusion-with-

binding results are more similar to the diffusion-only results than if this transition did not occur. This is because the fast dissociation of apotransferrin from the cell reduces the time transferrin is retained by a cell once bound (diffusion-with-binding model) or bound, internalized, and recycled (cellular pharmacology model). (Recall that the diffusion-with-binding case was calculated using the surface receptor number and dissociation rates experienced in the cellular pharmacology base case to allow a direct comparison of the models.) When the affinity is held constant, i.e., when $k_{ra} = k_{rd}$, there is a greater distinction between the diffusion-with-binding case and diffusion alone. Fig. 3, *d* and *e* give the spatial distribution of total transferrin for the three models with $K_A = 3 \times 10^7$ M^{-1} and 10^9 M^{-1}, respectively. The higher affinity might represent that of an antibody for its antigen. These panels show that both the cellular pharmacology and diffusion-with-binding models give higher peak transferrin concentrations and reduced penetration as affinity increases. However, the cellular pharmacology model still predicts the highest transferrin concentration at small r as well as the greatest reduction of penetration.

Parameter sensitivity analysis

In the study of parameter variation described below, we set $k_{ra} = k_{rd} = 1.667 \times 10^{-3}$ s^{-1} for all cases unless otherwise specified. This was necessary to observe the effects of the specific parameter variations listed without also varying the fraction of transferrin dissociating with the rate constants k_{ra} and k_{rd}.

Effects of diffusion coefficient (D) and initial drug concentration (L_0)

Increasing L_0 greatly increases the amplitude of the total transferrin (Tf_{tot}) profile in the tissue while the depth of penetration is relatively unaffected (Fig. 4a). This occurs because L_0 only multiplies temporal terms in Eq. 1, as well as scales the plasma concentration and capillary wall boundary condition. Conversely, increasing D results in a dramatic broadening and flattening of the total transferrin profile (Fig. 4 *b*). Increasing the value of the effective diffusivity represents either a molecule of smaller molecular weight or a tissue with less resistance to diffusion. Because the capillary permeability is not also changed to reflect alterations in molecular weight for these calculations, the plots in Fig. 4 *b* illustrate the latter case. Thus, the decreasing peak transferrin concentration and increasing tissue penetration associated with increasing diffusivity are caused by faster diffusion away from the blood vessel once the drug escapes the vessel. The results shown in Fig. 4 indicate that raising dosage (L_0) can affect tissue concentration but not depth of penetration under nonsaturating conditions. However, if effective diffusivity can be modified, the penetration depth of drug can be directly modulated. The effects of these parameters on intracellular transferrin concentration C_i and extracellular transferrin concentration L are similar to those for total transferrin concentration Tf_{tot} and hence are not shown.

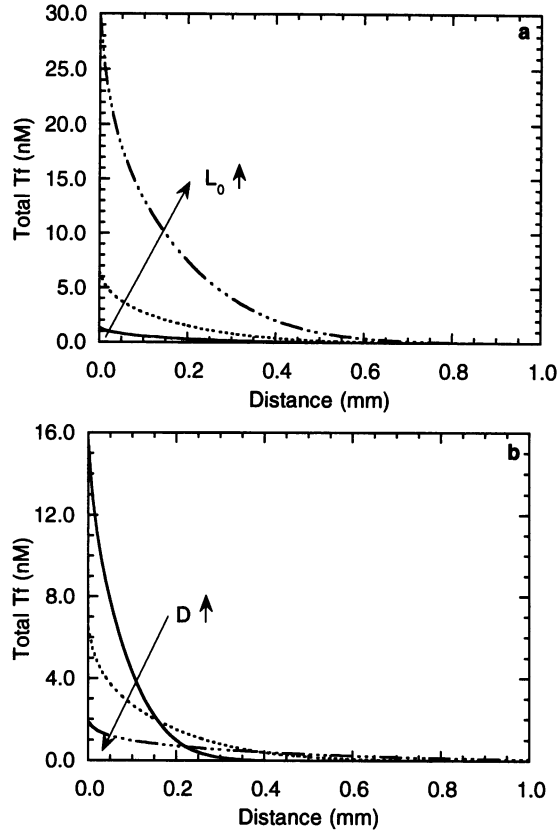

FIGURE 4 Effects of initial plasma transferrin concentration L_0 and effective diffusion coefficient D on spatial distribution of total transferrin Tf_{tot}. (*a*) Dependence on L_0: $L_0 = 4 \times 10^{-9}$, 2×10^{-8} (base case), and 10^{-7} M. (*b*) Dependence on D: $D = 4 \times 10^{-9}$, 2×10^{-8} (base case), and 10^{-7} cm^2 s^{-1}. Simulation time was 48 h. Similar trends are seen for all times compared up to 96 h.

Effects of recycling parameters (ff, $k_{rec,f}$, $k_{rec,s}$)

We considered the impact of the recycling parameters *ff*, $k_{rec,f}$, and $k_{rec,s}$ on the distribution of transferrin in the tissue. These parameters are grouped together in Eqs. 3–6, so varying any one is identical to varying the others proportionally. The effects are illustrated by varying $k_{rec,f}$. A fivefold increase or decrease of $k_{rec,f}$ from the base case value has negligible effects on both extracellular transferrin concentration L (Fig. 5, *solid curves*) and total transferrin concentration Tf_{tot} (Fig. 5, *dotted curves*). However, the intracellular concentration C_i (Fig. 5, *dashed curves*) decreases significantly as $k_{rec,f}$ increases. This occurs because increasing $k_{rec,f}$, $k_{rec,s}$, or *ff* effectively decreases transferrin cycle time, the time it takes for a transferrin molecule to traverse the entire internalization and recycling pathway. Hence, once internalized, a transferrin molecule is recycled more quickly to the cell surface for larger $k_{rec,f}$. The cell surface transferrin pool is simultaneously replenished, resulting in a nearly constant total cell-associated pool (not

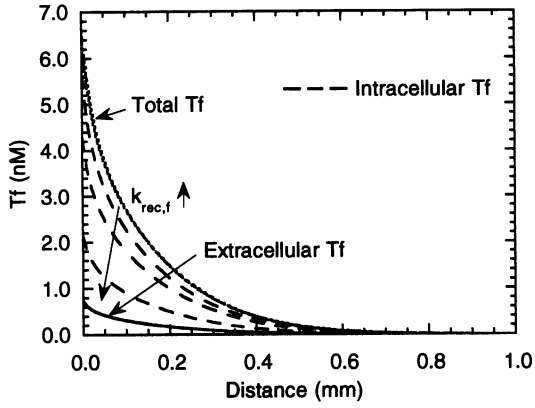

FIGURE 5 Effects of fast recycle rate constant $k_{rec,f}$. Spatial distribution of Tf_{tot}, L, and C_i at 48 h for $k_{rec,f} = 3.333 \times 10^{-4}$, 1.667×10^{-3} (base case), and 8.335×10^{-3} s^{-1}. Both total and extracellular profile dependence on $k_{rec,f}$ are given by sets of indistinguishable curves (*dotted* and *solid curves*, respectively).

shown). Thus, the only effect of varying recycle rate is to swap drug between cell surface and intracellular pools.

Effects of internalization parameter (k_{eR})

The effects of varying k_{eR} (internalization rate constant for receptor/transferrin complexes and free surface receptors) for the constant affinity system are shown in Fig. 6 *a*. Like the effects of $k_{rec,f}$ (Fig. 5), a 25-fold variation of k_{eR} has no appreciable effect on either the total (Tf_{tot}, Fig. 6 *a*, *dotted curves*) or extracellular (L, Fig. 6 *a*, *solid curves*) transferrin profiles. In contrast, intracellular transferrin concentration (C_i, Fig. 6 *a*, *dashed curves*) increases with increasing k_{eR} at all exposed r, while it decreases for the same variation of $k_{rec,f}$. Although increasing either parameter decreases the cycle time for a ligand, increasing k_{eR} also increases the likelihood that surface-bound transferrin will be internalized before it can dissociate and diffuse away (the rate of internalization is k_{eR} (C_{sa} + C_{sd}) while the rate of dissociation is k_{rd} (C_{sa} + C_{sd})). For the k_{eR} range studied ($k_{eR} = 6.667 \times 10^{-4}$ s^{-1} to 1.667×10^{-2} s^{-1}, with $k_{rd} = 1.667 \times 10^{-3}$ s^{-1}), this latter effect overwhelms the change in cycle time and results in the larger internal pool for larger k_{eR}.

This result is observed for the constant affinity case primarily because bound ligands are reinternalized and traverse the endocytic cycle several times before dissociation from the cell. In contrast, the variable affinity condition ($k_{ra} > k_{rd}$, the "true" transferrin system) causes nearly all apotransferrin to dissociate from the cell after one cycle, leaving little to be reinternalized. Because of this, varying k_{eR} has quite different effects in the variable affinity condition than in the more general constant affinity case described above (Fig. 6a). This is the only parameter that has a qualitatively different effect for the two conditions. The effects of k_{eR} for variable affinity conditions ($k_{ra} > k_{rd}$) are illustrated in Fig. 6, *b–d*. As k_{eR} increases, the amplitude of total transferrin concentration (Tf_{tot}) decreases while penetration depth increases (Fig. 6 *b*, *dotted curves*). Simultaneously, the penetration depth of extracellular transferrin L increases (Fig. 6 *b*, *solid curves*). Recall that Tf_{tot} and L are largely unaffected by changes in k_{eR} when affinity is constant (Fig. 6 *a*). An additional change is that the effect of increasing k_{eR} on intracellular transferrin (C_i) is biphasic

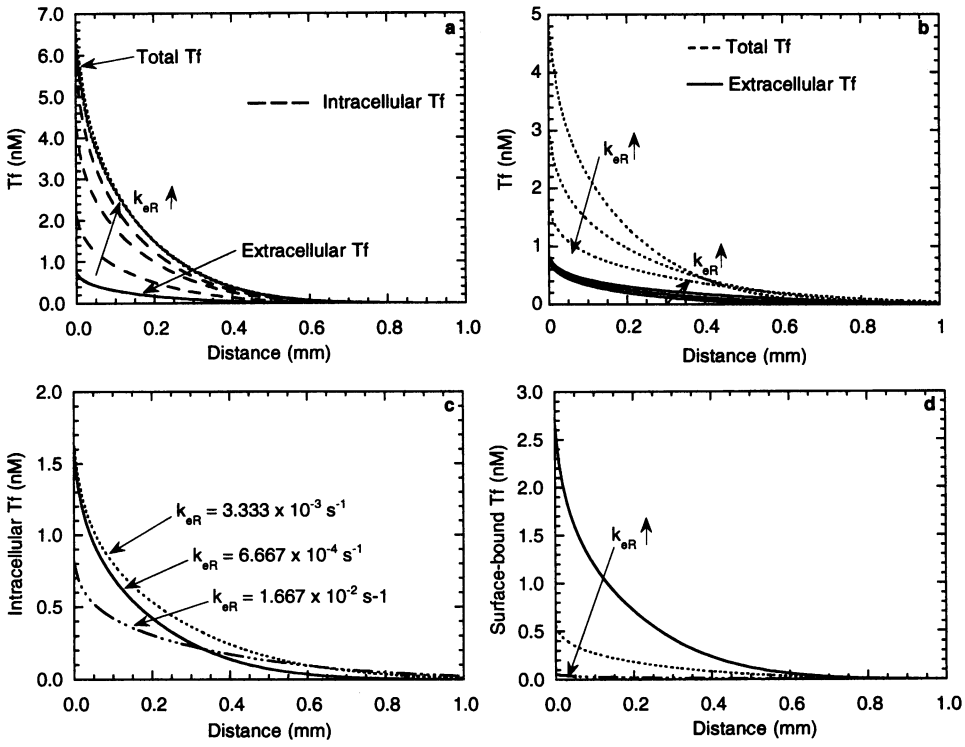

FIGURE 6 Effects of varying the internalization rate constant k_{eR} for (*a*) the constant affinity condition ($k_{ra} = k_{rd} = 1.667 \times 10^{-3}$ s^{-1}) and (*b–d*) the true transferrin case which has variable affinity ($k_{ra} > k_{rd}$). The values of k_{eR} used for the simulations in all panels are 6.667×10^{-4}, 3.333×10^{-3} (base case), and 1.667×10^{-2} s^{-1}, as indicated in the panels. Results are at 48 h. (*a*) Constant affinity condition. Spatial distributions of total tissue transferrin (Tf_{tot}), extracellular transferrin (L), and intracellular transferrin (C_i) concentrations. Varying k_{eR} has little effect on Tf_{tot} and L, which are given by sets of indistinguishable curves (*dotted* and *solid curves*, respectively). (*b–d*) True transferrin (variable affinity) condition. Spatial distributions of (*b*) Tf_{tot} (*dotted curves*) and L (*solid curves*), (*c*) C_i, and (*d*) cell surface transferrin (C_{sa} + C_{sd}) concentrations. The differences between the constant affinity and variable affinity cases are discussed in the text.

(Fig. 6 *c*), with an optimum intracellular distribution occurring when the base case value of k_{eR} is used. Increasing or decreasing k_{eR} causes a loss of amplitude or penetration depth, respectively. These results are caused by the combination of several cellular changes. First, the overall likelihood of internalization is decreased in comparison with the constant affinity case, because the net rate of transferrin dissociation (which now equals $k_{rd}\,C_{sd} + k_{ra}\,C_{sa}$; $k_{ra} > k_{rd}$) is now much faster than the rate of internalization (k_{eR} ($C_{sd} + C_{sa}$)); bound transferrin cycles through the cell only once before fast dissociation as apotransferrin. This is true for the entire range of k_{eR} studied, because k_{eR} is much smaller than k_{ra}. Second, in the variable affinity case, increasing k_{eR} shortens the cycle time at both the internalization step and the dissociation step (because of the diferric to apotransferrin transition that occurs during recycle). Third, there is a shift of free receptors from the surface to inside the cell as k_{eR} increases. This reduces the ability of the cell to capture free extracellular transferrin, resulting in a large decrease in cell surface complexes with increasing k_{eR} (Fig. 6 *d*). The biphasic variation in intracellular concentration with k_{eR} (Fig. 6 *c*) is the result of a tradeoff between the changes in cycle time and internalizable surface complex concentration described above. Extracellular transferrin penetrates to greater depths with increasing k_{eR} because less is captured by the cells, owing to fewer cell surface receptors (Fig. 6 *b*). The sum of the effects on the intracellular, cell surface, and extracellular pools results in increased penetration but decreased maximum amplitude in the total tissue transferrin profile (Fig. 6 *b*).

Effects of binding parameters (k_f, k_{rd})

The effects of binding rates on the distribution of transferrin in tissue were examined by varying the binding rate parameters k_f and k_{rd}. The effects of k_f on total (Tf_{tot}), intracellular (C_i), and extracellular (L) transferrin concentrations at 48 h are plotted versus distance in Fig. 7. Tf_{tot} and C_i increase dramatically in amplitude but decrease in penetration depth (Fig. 7, *a* and *b*) with increasing k_f. In contrast, L profiles (Fig. 7 *c*) show decreasing penetration depth without appreciable change in maximal amplitude as k_f increases (note differences in scale on the ordinates). This result occurs because faster binding (k_f increasing) with subsequent internalization causes more cell-associated transferrin and creates a larger intracellular transferrin pool while depleting the extracellular pool. This is further illustrated by the effect of k_f on the partitioning of transferrin among intracellular (C_i), extracellular (L), and total cell-associated (Tf_{tca}) pools (Fig. 8). Fig. 8 *a* shows that when k_f is low (10^4 M^{-1} s^{-1}) much of the transferrin in the tissue is extracellular. However, when k_f is high (2.5×10^5 M^{-1} s^{-1}), most of the transferrin is intracellular (Fig. 8 *b*) (note differences in scale on the ordinates). A striking difference between the two panels is that the penetration of transferrin is much greater for low k_f than for high k_f. Because cells retain higher intracellular concentrations of transferrin as k_f increases, the cell plasma membrane represents a physical barrier to transferrin penetration into the tissue. We refer to this phenomenon as "internal trapping."

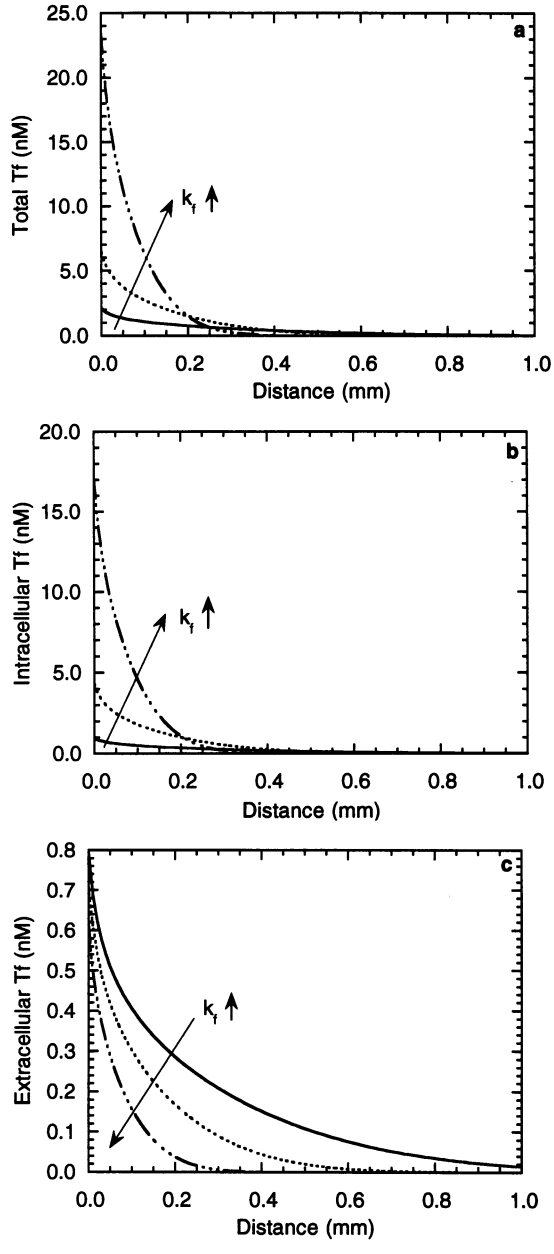

FIGURE 7 Effects of forward binding rate constant k_f. Dependence of spatial distribution of (*a*) total transferrin Tf_{tot}, (*b*) intracellular transferrin C_i, and (*c*) extracellular transferrin L at 48 h; $k_f = 10^4$, 5×10^4 (base case), and 2.5×10^5 M^{-1} s^{-1}.

The effects of k_{rd} are similar (although opposite in direction) to those presented for k_f in Figs. 7 and 8, and so the simulations are not shown. The effects of binding parameters are often analyzed in terms of the affinity constant K_A, the ratio of forward and reverse binding rate constants. Clearly, the effects of affinity on transferrin distribution in tissue are implied by the effects of k_f just discussed and were also shown in Fig. 3, *d* and *e*. In this study, the

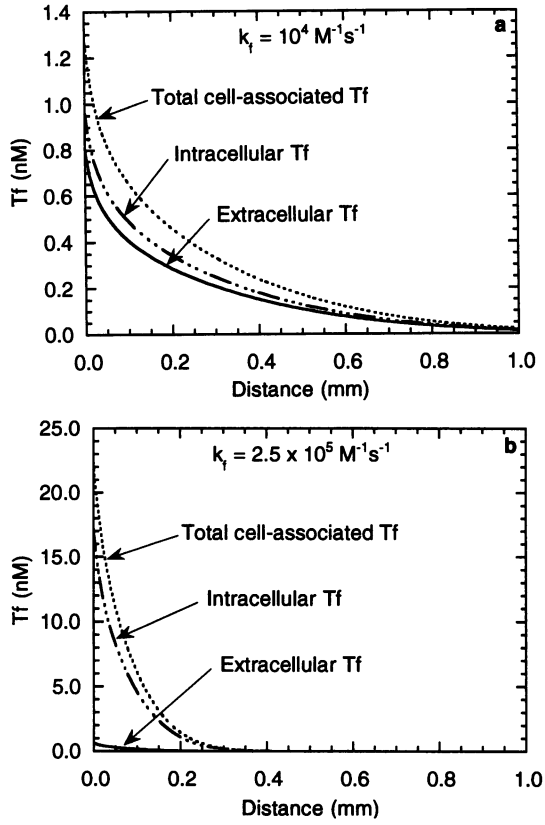

FIGURE 8 Effect of forward binding rate constant k_f on partitioning of transferrin among extracellular (L), intracellular (C_i), and total cell-associated (Tf_{tca}) pools. Recall that Tf_{tca} is the sum of intracellular and surface-bound transferrin. Spatial distributions at 48 h are shown for (*a*) $k_f = 10^4$ M^{-1} s^{-1} and (*b*) $k_f = 2.5 \times 10^5$ M^{-1} s^{-1}. Note the different scales on the ordinates of (*a*) and (*b*). This result demonstrates that decreased penetration of transferrin is caused by the internalization of transferrin.

maximum free transferrin concentration observed ($L = 4.6 \times 10^{-9}$ M; data not shown) is lower than the dissociation constant K_D ($=1/K_A$), illustrating that we have considered unsaturated conditions in all cases.

Effects of receptor density parameters (R_T, n_v)

Receptor density can be modified either by changing the total number of receptors per cell (R_T) or the cell number density (n_v), although the latter might also alter the effective diffusion coefficient. Average total, intracellular, and extracellular transferrin concentrations all depend on receptor density and closely parallel the behavior shown for variation of affinity described above, and hence the simulations are not shown. At all times, the dependence of total transferrin concentration Tf_{tot} on receptor density is similar to that seen for intracellular transferrin concentration C_i. Increasing receptor density results in an increased amplitude of Tf_{tot} and C_i that coincides with reduced penetration depth. Comparison of partitioning of transferrin among intracellular, extracellular, and total cell-associated pools for high receptor density and low receptor density demonstrates the internal trapping phenomenon as illustrated in Fig. 8 for variations in k_f. This occurs because increased receptor density results in greater capture of transferrin and leads to decreased penetration of extracellular transferrin in conjunction with greatly increased amplitude of intracellular transferrin concentration C_i.

DISCUSSION

We have developed a mathematical model for the transport and distribution of macromolecular drugs in physiological tissues. The model, referred to as the cellular pharmacology model, includes diffusion of drug in the extracellular space, reversible binding of drug to cell surface receptors, and internalization and intracellular trafficking of drug by cells. This detailed consideration of cellular pharmacology distinguishes our model from previous models that either neglected cellular internalization and routing of drug or lumped these processes and described them with a single rate constant. In this paper, we present results for the distribution of transferrin in a tissue expressing the transferrin receptor. However, the model is easily applied to any drug/receptor system or tissue type for which the required parameter values are known. Note that all parameter values used in these simulations are for native transferrin as the ligand. Clearly, rate constants might be different for transferrin conjugated to a therapeutic agent.

The effectiveness of a targeted therapeutic agent depends on both its potency and its access to the tissue of interest. In addition, cellular interactions with a targeting drug greatly influence drug potency. There is abundant evidence that the strength of drugs such as immunotoxins containing protein-synthesis inhibitors or oligonucleotides for gene therapy is related to the respective rates of internalization and degradation of these drugs (Byers et al., 1991; Wargalla and Reisfeld, 1989) as well as to the particular intracellular routing pathway through which they are directed (May et al., 1991; Chignola et al., 1990). Further, Mattes et al. (1994) have recently suggested that internalization of radiolabeled antibodies may improve the cytotoxicity of these drugs if the radioisotopes are retained within cells. There is no consensus, however, as to which cellular drug processing step is most important in determining therapeutic effect. Clearly, drug delivery strategies must be designed to optimize cellular behavior based on the therapeutic goal, e.g., cell toxicity versus gene therapy. While drug/cell interactions are critical to drug potency, these same processes may also affect drug access to the tissue of interest. For example, immunotoxins have been observed to distribute nonuniformly in vitro (Sutherland et al., 1987; Kikuchi et al., 1992) and in vivo (Juweid et al., 1992; Sung et al., 1993). To explain this nonuniformity, mathematical analyses of the distribution of macromolecular drugs have identified contributing factors such as interstitial pressure gradients (Baxter and Jain, 1991) and the "binding site barrier" (van Osdol et al., 1991). However, these models also implied that the

heterogeneity of the spatial distribution of drug would be increased by drug interactions with cells.

We developed the cellular pharmacology model to test the hypothesis that cellular processing of a drug influences its distribution in a tissue. We compared the distribution of transferrin predicted by the cellular pharmacology model with those predicted by simpler models that considered either extracellular diffusion of transferrin alone, or extracellular diffusion and reversible binding of transferrin to cell surface receptors. The results show that the penetration of transferrin is compromised by the addition of rate processes associated with transferrin/cell interactions. The total amount of transferrin in the tissue close to the source increases, however, because much is internalized by the cells. These results also demonstrate that models that do not include intracellular trafficking greatly underestimate the uptake and retention of drug in a tissue. To examine whether the observed differences among models were significant for different receptor/ligand affinities, we compared the distribution of transferrin predicted by the three models for constant diferric transferrin affinity ($k_{ra} = k_{rd} = 1.667 \times 10^{-3}$ s^{-1}) to that given by a higher, antibody-like affinity (Fig. 3, *d* and *e*). The results show that the differences between the cellular pharmacology model and the diffusion with binding model are applicable to and exaggerated for higher affinity receptor/ligand systems.

The cellular pharmacology model provides an initial evaluation of the potential effects of cellular pharmacology on drug distribution in a tissue where diffusive transport occurs, and it has some limitations. The tissue is modeled as a homogeneous continuum, and an effective diffusion coefficient is used to account for the tissue porosity and architecture. Additional means of transport such as convection, intracellular diffusion, and directed vesicular transport within cells have been neglected, but may be important in certain tissue types. We have also neglected the possibility of extracellular sinks for drug such as degradation, lymphatic uptake, and nonspecific binding to extracellular matrix elements. On the other hand, we have found that the results presented here, in terms of the effects of cellular pharmacology on drug transport, are qualitatively the same for a number of different boundary conditions (constant drug concentration at $r = 0$, time-dependent drug concentration at $r = 0$ as reported here, varying capillary permeability, no drug at $r = \infty$) and tissue geometries (planar, cylindrical) (results not shown).

We have examined the sensitivity of the cellular pharmacology model results to key parameters to investigate how one might try to modulate drug delivery by modifying cell/drug interactions. Our analyses indicate that increasing dosage (L_0) can affect tissue concentration of drug but not depth of penetration under nonsaturating conditions. In contrast, penetration depth of drug can be directly modulated by modifying the effective diffusivity. We also find that varying the binding and trafficking rate parameters affects several cell characteristics including cell surface receptor number, likelihood of internalization of bound ligand, and endocytic cycle time. Results of variation of recycling and internalization parameters ($k_{rec,f}$, $k_{rec,s}$, *ff*, and k_{eR}) illustrate that one might dramatically alter the intracellular exposure to drug without significantly affecting the total or extracellular drug distribution. These results indicate that modifying the recycling and internalization parameters may influence the efficacy of drugs that must act intracellularly. Changes in binding parameters that mimic an increase in affinity (e.g., increasing k_f or decreasing k_{rd}) or, alternatively, increases in receptor density via R_T or n_v, cause a pronounced translocation of transferrin from outside cells to mostly inside cells; this leads to a reduction of transferrin penetration into the tissue. Thus, there may be a trade-off between homogeneity of drug distribution and intracellular exposure to drug.

An important aspect of the transferrin cycle is the transition of transferrin from the diferric state to the apo state as a result of internalization and recycle. This transition causes a large fraction of the cell-associated transferrin (that which is internalized and recycled) to dissociate from receptors at an increased rate versus diferric transferrin. Although this phenomenon is essential to an accurate model of the transferrin cycle, its inclusion in our model introduces ambiguity in the interpretation of the results of parameter sensitivity analyses, as it is not possible to vary most parameters without also varying the fraction of transferrin dissociating with k_{ra} compared with k_{rd}. For this reason, we performed all parameter variations with $k_{ra} = k_{rd}$ (Figs. 4–8). This modification both ensures the clarity of interpretation of our results and helps to generalize the cellular pharmacology model results to ligands other than transferrin. The results calculated with constant affinity (Figs. 3, *d* and *e*, and 4–8) illustrate that the influence of cellular pharmacology is not limited to the transferrin system but is a phenomenon common to systems in which receptors and receptor/ligand complexes are internalized. The true transferrin system ($k_{ra} > k_{rd}$) approximates the case in which receptor and ligand dissociate in the endosome and recycled free ligand returns directly to the extracellular space, while the $k_{ra} = k_{rd}$ system represents the case in which receptor and ligand remain associated in the endosome and recycled ligand undergoes a membrane dissociation event before returning to the extracellular space. It was noteworthy to find that the results for the true transferrin system were qualitatively the same as the $k_{ra} = k_{rd}$ results for variation of all parameters except k_{eR}. This finding illustrates the broad applicability of the results presented here. Another aspect of the model specific to the transferrin system is the slow recycle pathway. This pathway contributes very little to the retention of transferrin by cells for the value of $k_{rec,s}$ used, however, and there would be no significant change in the results if the slow pathway were not included (results not shown).

The cellular pharmacology model provides a distribution of intracellular drug concentration, an important piece of information that is lacking in other drug distribution models. Interestingly, the cellular pharmacology model predicts that most of the transferrin present in the model tissue after

very early times is intracellular and thus unable to penetrate to greater tissue depths. This indicates that the observed nonuniform distributions of targeting drugs may be caused mainly by intracellular containment, or "internal trapping." In contrast, the diffusion-with-surface-binding model predicts that penetration of drug is impeded because of specific binding of drug to cell surface receptors. This result was described as a binding site barrier by Fujimori et al. (1989). Experimental support for the binding site barrier hypothesis was provided by Juweid et al. (1992), who observed that heterogeneous distribution of monoclonal antibodies in guinea pig carcinomas corresponded to antigen location. These investigators inferred that a binding site barrier was responsible for low antibody penetration. Pervez et al. (1988) and Shockley et al. (1992a) found similar behavior of monoclonal antibodies in LoVo xenografts and human melanoma xenografts, respectively. The above studies clearly distinguished between extracellular antibody and cell-associated antibody, but the distinction between surface-bound antibody and intracellular antibody was either not discernible or not investigated. The concept of internal trapping of drug extends the binding site barrier theory; because receptor-mediated internalization requires specific binding of drug to cell surface receptors, the two are necessarily related.

The internal trapping phenomenon is clearly illustrated by the sensitivity of the cellular pharmacology model to changes in receptor density and receptor/transferrin affinity. Weinstein et al. (1987) and Fujimori et al. (1989) observed in modeling studies that the barrier to drug penetration grew in proportion to increases in these parameters. We observe a similar result in that the distribution of transferrin throughout the model tissue is increasingly nonuniform as receptor density or receptor/transferrin affinity increases. However, in our system, the reduced penetration of transferrin is a result of the intracellular containment that follows surface binding and not surface binding in and of itself. A key contrast between the consequences of the binding site barrier theory and the concept of internal trapping is the following. Out of the context of intracellular drug distributions, one might speculate that increased cell surface retention of drug leads to less uniform drug distribution and hence submaximal drug efficacy. Our results show that, for drugs that require internalization for activity, parameter changes that enhance intracellular drug retention while decreasing extracellular drug penetration may make positive contributions to drug efficacy.

It is necessary to note that internalization alone of targeted therapeutics is not a guarantee of drug efficacy. The mechanisms of action of many drugs require access to the cytosol or nucleus. Because the details of the intracellular routing associated with drug action are often not well characterized, we have not accounted for this aspect of drug efficacy. Rather, we have examined the total internalization of transferrin with the presumption that some fraction of the intracellular drug will have the desired effect.

We tested the sensitivity of the cellular pharmacology model to parameters that control the rates of internalization and intracellular routing of transferrin. The results show that total drug content in a tissue is not a sufficient indicator of therapeutic effect for drugs that require intracellular access for activity. For instance, we observed that large changes in the rate of recycle of transferrin and in the fraction of transferrin recycled in the fast pathway had dramatic effects on the intracellular transferrin concentration profiles but did not significantly affect total transferrin concentration in the tissue. Similar results were seen for variation of the internalization rate constant. Hence, it may be possible to optimize the intracellular drug concentration without altering the extracellular and total drug profiles simply by modulating cellular drug processing parameters. In addition, these results show that total tissue drug content can be misleading if the goal is to predict intracellular concentration response to parameter changes by studying the response of total drug concentration. The effects of cellular drug processing parameters on transferrin distribution indicate that maximal tissue content may not reflect optimal effectiveness of treatment. These results are important in light of the fact that total tissue drug content is a commonly measured indicator of the successful delivery, and hence efficacy, of targeted drugs. Temporal profiles of average total drug concentration in a tissue (Langmuir et al., 1992; Shockley et al., 1992b; van Osdol et al., 1991) are used as measures of average tissue exposure to drug, while spatial profiles of total drug concentration (Sung et al., 1993; van Osdol et al., 1991; Baxter et al., 1992) illustrate which areas of the tissue have been exposed to the drug and the extent of the exposure. However, as the cellular pharmacology model demonstrates, important information about drug location with respect to individual cells (e.g., intracellular versus extracellular) is lost in a measure of total drug concentration.

Our results illustrate that specific transferrin/cell interactions can have a significant impact on the distribution of transferrin throughout a model tissue. From this specific application, we can generalize and predict that cellular pharmacology is likely to influence the distribution, and hence efficacy, of any targeted drug. Models such as ours that incorporate cellular pharmacology should be beneficial in identifying key processes and rate-limiting steps that govern drug distribution in a particular tissue, and hence can be useful tools for the rational design of drugs. In addition, such models can be used to provide detailed tissue-level input to pharmacokinetic analyses of whole-body drug distribution. To these ends, future work needs to examine the cellular pharmacology/transport behavior for different ligand/receptor systems (e.g., epidermal growth factor and its receptor, anti-transferrin receptor antibody/transferrin receptor), different cell types, and different drug delivery protocols (e.g., two-step antibody therapy) to determine the impact of drug/cell interactions on the distribution of these ligands.

We gratefully acknowledge helpful discussions with Richard Willson. This work was funded by a National Science Foundation Presidential Young Investigator Award (BCS-9157783) and grants from the University of Houston Institute for Space Systems Operations to C. L. S. and an NSF Graduate Research Fellowship to R. K. R.

REFERENCES

Akhtar, S., and R. L. Juliano. 1992. Cellular uptake and intracellular fate of antisense oligonucleotides. *Trends Cell Biol.* 2:139–145.

Baxter, L. T., and R. K. Jain. 1991. Transport of fluid and macromolecules in tumors III: role of binding and metabolism. *Microvasc. Res.* 41:5–23.

Baxter, L. T., F. Yuan, and R. K. Jain. 1992. Pharmacokinetic analysis of the perivascular distribution of bifunctional antibodies and haptens: comparison with experimental data. *Cancer Res.* 52:5838–5844.

Boucher, Y., L. T. Baxter, and R. K. Jain. 1990. Interstitial pressure gradients in tissue-isolated and subcutaneous tumors: implications for therapy. *Cancer Res.* 50:4478–4484.

Byers, V. S., I. Z. A. Pawluczyk, D. S. W. Hooi, M. R. Price, S. Carroll, M. J. Embleton, M. C. Garnett, N. Berry, R. A. Robins, and R. W. Baldwin. 1991. Endocytosis of immunotoxin-79IT/36-RTA by tumor cells in relation to its cytotoxic action. *Cancer Res.* 51:1990–1995.

Cain, C. C., R. B. Wilson, and R. F. Murphy. 1991. Isolation by fluorescence-activated cell sorting of Chinese hamster ovary cell lines with pleiotropic temperature-conditional defects in receptor recycling. *J. Biol. Chem.* 266:11746–11752.

Chen, J., S. Gamou, A. Takayanagi, and N. Shimizu. 1994. A novel gene delivery system using EGF receptor-mediated endocytosis. *FEBS Lett.* 338:167–169.

Chignola, R., M. Colombatti, L. Dell'Archiprete, C. Candiani, and G. Tridente. 1990. Distribution of endocytosed molecules to intracellular acidic environments correlates with immunotoxin activity. *Int. J. Cancer.* 46:1117–1123.

Ciechanover, A., A. L. Schwartz, A. Dautry-Varsat, and H. F. Lodish. 1983. Kinetics of internalization and recycling of transferrin and the transferrin receptor in a human hepatoma cell line. *J. Biol. Chem.* 258:9681–9689.

Citro, G., D. Perrotti, C. Cucco, I. D'Agnano, A. Sacchi, G. Zupi, and B. Calabretta. 1992. Inhibition of leukemia cell proliferation by receptor-mediated uptake of c-*myb* antisense oligodeoxynucleotides. *Proc. Natl. Acad. Sci. USA.* 89:7031–7035.

Cotten, M., F. Langle-Rouault, H. Kirlappos, E. Wagner, K. Mechtler, M. Zenke, H. Beug, and M. L. Birnstiel. 1990. Transferrin-polycation-mediated introduction of DNA into human leukemic cells: stimulation by agents that affect the survival of transfected DNA or modulate transferrin receptor levels. *Proc. Natl. Acad. Sci. USA.* 87:4033–4037.

Dautry-Varsat, A., A. Ciechanover, and H. F. Lodish. 1983. pH and the recycling of transferrin during receptor-mediated endocytosis. *Proc. Natl. Acad. Sci. USA.* 80:2258–2262.

Davis, M. E. 1984. Numerical Methods and Modeling for Chemical Engineers. John Wiley and Sons, New York.

Epstein, A. L., and L. A. Khawli. 1991. Tumor biology and monoclonal antibodies: overview of basic principles and clinical considerations. *Antibodies Immunoconjugates Radiopharm.* 4:373–384.

Firestone, R. A. 1994. Low-density lipoprotein as a vehicle for targeting antitumor compounds to cancer cells. *Bioconjugate Chem.* 5:105–113.

Fujimori, K., D. G. Covell, J. E. Fletcher, and J. N. Weinstein. 1989. Modeling analysis of the global and microscopic distribution of immunoglobulin G, $F(ab')_2$, and Fab in tumors. *Cancer Res.* 49:5656–5663.

Hirota, N., M. Ueda, S. Ozawa, O. Abe, and N. Shimizu. 1989. Suppression of an epidermal growth factor receptor-overproducing tumor by an immunotoxin conjugate of gelonin and a monoclonal anti-epidermal growth factor receptor antibody. *Cancer Res.* 49:7106–7109.

Jain, R. K. 1989. Delivery of novel therapeutic agents in tumors: physiological barriers and strategies. *J. Natl. Cancer Inst.* 81:570–576.

Jain, R. K. 1990. Physiological barriers to delivery of monoclonal antibodies and other macromolecules in tumors. *Cancer Res.* 50(Suppl.): 814–819.

Jain, R. K. 1994. Barriers to drug delivery in solid tumors. *Sci. Am.* 270:58–65.

Juweid, M., R. Neumann, C. Paik, M. J. Perez-Bacete, J. Sato, W. van Osdol, and J. N. Weinstein. 1992. Micropharmacology of monoclonal antibodies in solid tumors: direct evidence for a binding site barrier. *Cancer Res.* 52:5144–5153.

Karin, M., and B. Mintz. 1981. Receptor-mediated endocytosis of transferrin in developmentally totipotent mouse teratocarcinoma stem cells. *J. Biol. Chem.* 256:3245–3252.

Kikuchi, T., T. Ohnuma, J. F. Holland, and L. E. Spitler. 1992. Penetration of anti-melanoma immunotoxin into multicellular tumor spheroids and cell kill effects. *Cancer Immunol. Immunother.* 35:302–306.

Kim, K. J., B. Li, J.. Winer, M. Armanini, N. Gillett, H. S. Phillips, and N. Ferrara. 1993. Inhibition of vascular endothelial growth factor-induced angiogenesis suppresses tumor growth in vivo. *Nature.* 362:841–844.

Klausner, R. D., G. Ashwell, J. van Renswoude, J. B. Harford, and K. R. Bridges. 1983. Binding of apotransferrin to K652 cells: explanation of the transferrin cycle. *Proc. Natl. Acad. Sci. USA.* 80:2263–2266.

Klausner, R. D., J. van Renswoude, C. Kempf, K. Rao, J. L. Bateman, and A. R. Robbins. 1984. Failure to release iron from transferrin in a Chinese hamster ovary cell mutant pleiotropically defective in endocytosis. *J. Biol. Chem.* 98:1098–1101.

Langmuir, V. K., H. L. Mendonca, and D. V. Woo. 1992. Comparisons between two monoclonal antibodies that bind to the same antigen but have differing affinities: uptake kinetics and ^{125}I-antibody therapy efficacy in multicell spheroids. *Cancer Res.* 52:4728–4734.

Lauffenburger, D. A., and J. J. Linderman. 1993. Receptors: Models for Binding, Trafficking, and Signaling. Oxford University Press, New York.

Leichner, P. K., N. C. Yang, B. W. Wessels, W. G. Hawkins, S. E. Order, and J. L. Klein. 1990. Dosimetry and treatment planning in radioimmunotherapy. *Front. Radiat. Ther. Oncol.* 24:109–122.

LoBuglio, A. F. and M. N. Saleh. 1992. Advances in monoclonal antibody therapy of cancer. *Am. J. Med. Sci.* 304:214–224.

Martell, L. A., A. Agrawal, D. A. Ross, and K. M. Muraszko. 1993. Efficacy of transferrin receptor-targeted immunotoxins in brain tumor cell lines and pediatric brain tumors. *Cancer Res.* 53:1348–1353.

Mattes, M. J., G. L. Griffiths, H. Diril, D. M. Goldenberg, G. L. Ong, and L. B. Shih. 1994. Processing of antibody-radioisotope conjugates after binding to the surface of tumor cells. *Cancer.* 73:787–793.

May, R. D., H. T. Wheeler, F. D. Finkelman, J. W. Uhr, and E. S. Vitetta. 1991. Intracellular routing rather than cross-linking or rate of internalization determines the potency of immunotoxins directed against different epitopes of sIgD on murine B cells. *Cell. Immunol.* 135:490–500.

McCabe, W. L., J. C. Smith, and P. Harriott. 1985. Unit Operations of Chemical Engineering, 4th ed. McGraw-Hill, Inc., New York.

McFadden, R., and C. S. Kwok. 1988. Mathematical model of simultaneous diffusion and binding of antitumor antibodies in multicellular human tumor spheroids. *Cancer Res.* 48:4032–4037.

Mulshine, J. L., N. Shuke, F. Daghighian, J. Carrasquillo, B. Ghosh, T. Walsh, I. Avis, J. C. Reynolds, F. Cuttitta, and S. M. Larson. 1992. The correct dose: pharmacologically guided end point for anti-growth factor therapy. *Cancer Res.* 52(Suppl.):2743–2746.

Olsnes, S., K. Sandvig, O. W. Petersen, and B. van Deurs. 1989. Immunotoxins: entry into cells and mechanisms of action. *Immunol. Today.* 10:291–295.

Pervez, S., A. A. Epenetos, W. J. Mooi, D. J. Evans, G. Rowlinson, B. Dhokia, and T. Krausz. 1988. Localization of monoclonal antibody AUA1 and its $F(ab')_2$ fragments in human tumor xenografts: an autoradiographic and immunohistochemical study. *Int. J. Cancer.* 3(Suppl.): 23–29.

Pirker, R., D. J. P. FitzGerald, T. C. Hamilton, R. F. Ozols, M. C. Willingham, and I. Pastan. 1985. Anti-transferrin receptor antibody linked to *Pseudomonas* exotoxin as a model immunotoxin in human ovarian carcinoma cell lines. *Cancer Res.* 45:751–757.

Preijers, F. W. M. B., W. J. M. Tax, T. DeWitte, A. Janssen, H. V. D. Heidjen, H. Vidal, J. M. C. Wessels, and P. J. A. Capel. 1988. Relationship between internalization and cytotoxicity of ricin A-chain immunotoxins. *Br. J. Haematol.* 70:289–294.

Press, W. H., B. P. Flannery, S. A. Teukolsky, and W. T. Vetterling. 1989. Numerical Recipes: The Art of Scientific Computing (FORTRAN version). Cambridge University Press, New York.

Schwartz, J., B. Penke, J. Rivier, and W. Vale. 1987. A new cytotoxin specific for the target cells of corticotropin-releasing factor. *Endocrinology.* 121:1454–1460.

Shockley, T. R., K. Lin, J. A. Nagy, R. G. Tompkins, M. L. Yarmush, and H. F. Dvorak. 1992a. Spatial distribution of tumor-specific monoclonal antibodies in human melanoma xenografts. *Cancer Res.* 52:367–376.

Shockley, T. R., K. Lin, C. Sung, J. A. Nagy, R. G. Tompkins, R. L. Dedrick, and H. F. Dvorak. 1992b. A quantitative analysis of tumor specific monoclonal antibody uptake by human melanoma xenografts: effects of antibody immunological properties and tumor antigen expression levels. *Cancer Res.* 52:357–366.

Stein, C. A. and Y.-C. Cheng. 1993. Antisense oligonucleotides as therapeutic agents: is the bullet really magical? *Science.* 261:1004–1012.

Sung, C., R. L. Dedrick, W. A. Hall, P. A. Johnson, and R. J. Youle. 1993. The spatial distribution of immunotoxins in solid tumors: assessment by quantitative autoradiography. *Cancer Res.* 53:2092–2099.

Sung, C., T. R. Shockley, P. F. Morrison, H. F. Dvorak, M. L. Yarmush, and R. L. Dedrick. 1992. Predicted and observed effects of antibody affinity and antigen density on monoclonal antibody uptake in solid tumors. *Cancer Res.* 52:377–384.

Sutherland, R., F. Buchegger, M. Schreyer, A. Vacca, and J-P. Mach. 1987. Penetration and binding of radiolabeled anti-carcinoembryonic antigen monoclonal antibodies and their antigen binding fragments in human colon multicellular tumor spheroids. *Cancer Res.* 47:1627–1633.

Thomas, G. D., M. J. Chappell, P. W. Dykes, D. B. Ramsden, K. R. Godfrey, J. R. M. Ellis, and A. R. Bradwell. 1989. Effect of dose, molecular size, affinity, and protein binding on tumor uptake of antibody or ligand: a biomathematical model. *Cancer Res.* 49: 3290–3296.

Thorstensen K. and I. Romslo. 1993. The transferrin receptor: its diagnostic value and its potential as therapeutic target. *Scand. J. Clin. Lab. Invest.* 53 (Suppl. 215):113–120.

van Osdol, W., K. Fujimori, and J. N. Weinstein. 1991. An analysis of monoclonal antibody distribution in microscopic tumor nodules: consequences of a "binding site barrier". *Cancer Res.* 51:4776–4784.

van Osdol, W. W., C. Sung, R. L. Dedrick, and J. N. Weinstein. 1993. A distributed pharmacokinetic model of two-step imaging and treatment protocols: application to streptavidin-conjugated monoclonal antibodies and radiolabeled biotin. *J. Nucl. Med.* 34:1552–1564.

Vitetta, E. S., P. E. Thorpe, and J. W. Uhr. 1993. Immunotoxins: magic bullets or misguided missiles? *Immunol. Today.* 14:252–259.

Wargalla, U. C. and R. A. Reisfeld. 1989. Rate of internalization of an immunotoxin correlates with cytotoxic activity against human tumor cells. *Proc. Natl. Acad. Sci. USA.* 86:5146–5150.

Weinstein, J. N., R. R. Eger, D. G. Covell, C. D. V. Black, J. Mulshine, J. A. Carrasquillo, S. M. Larson, and A. M. Keenan. 1987. The pharmacology of monoclonal antibodies. *Ann. NY Acad. Sci.* 507:199–210.

Yoshikawa, T., and W. M. Pardridge. 1992. Biotin delivery to brain with a covalent conjugate of avidin and a monoclonal antibody to the transferrin receptor. *J. Pharmacol. Exp. Ther.* 263:897–903.